Pediatr Radiol (2017) 47:522–533
DOI 10.1007/s00247-017-3778-0

MINISYMPOSIUM: MR TECHNIQUES IN PEDIATRIC RADIOLOGY

Advanced imaging techniques in pediatric body MRI

Jesse Courtier[1] · **Anil G. Rao**[2] · **Sudha A. Anupindi**[3]

Received: 13 September 2016 / Revised: 19 November 2016 / Accepted: 3 January 2017 / Published online: 12 April 2017

Abstract While there are many challenges specific to pediatric abdomino-pelvic MRI, many recent advances are addressing these challenges. It is therefore essential for radiologists to be familiar with the latest advances in MR imaging. Laudable efforts have also recently been implemented in many centers to improve the overall experience of pediatric patients, including the use of dedicated radiology child life specialists, MRI video goggles, and improved MR suite environments. These efforts have allowed a larger number of children to be scanned while awake, with fewer studies being done under sedation or anesthesia; this has resulted in additional challenges from patient motion and difficulties with breath-holding and tolerating longer scan times. In this review, we highlight common challenges faced in imaging the pediatric abdomen and pelvis and discuss the application of the newest techniques to address these challenges. Additionally, we highlight the newest advances in quantified imaging techniques, specifically in MR liver iron quantification. The techniques described in this review are all commercially available and can be readily implemented.

Keywords Abdomen · Body · Children · Magnetic resonance imaging · Motion correction · Techniques

✉ Jesse Courtier
jesse.courtier@ucsf.edu

[1] Department of Radiology and Biomedical Imaging, UCSF Benioff Children's Hospital, 1975 4th St., C1785L, San Francisco, CA 94158, USA

[2] Department of Radiology, Medical University of South Carolina, Charleston, SC, USA

[3] Department of Radiology, Children's Hospital of Philadelphia, Philadelphia, PA, USA

Introduction

Although there are many challenges specific to pediatric abdomino-pelvic magnetic resonance imaging (MRI), many recent advances have been made to address these challenges. MRI is being increasingly used in assessment of pediatric patients, and it is therefore essential for radiologists to be familiar with the latest advances in MR imaging [1]. Many centers have implemented measures to improve the overall experience of pediatric patients, including the use of dedicated radiology child life specialists, MRI video goggles, and improved environments such as the GE Adventure Series (GE Healthcare, Waukesha, WI) and Philips Ambient Experience (Philips Healthcare, Best, The Netherlands) [2–5]. These efforts have allowed a larger portion of children to be scanned while awake, with fewer studies being done under sedation or anesthesia; this in turn has resulted in additional challenges of patient motion, breath-holding, and tolerating longer scan times.

In this review, we highlight common challenges faced in imaging the pediatric abdomen and pelvis and discuss how the newest techniques address these challenges. Additionally we highlight the newest advances in quantified imaging techniques, specifically in MR liver iron quantification. The techniques described in this review are all commercially available and can be readily implemented. We have summarized the key applications of these sequences in the provided table (Table 1).

Motion correction techniques

The environmental factors of a small confined space, loud noise of the MRI scanner, and an unfamiliar setting are significant sources of anxiety in pediatric patients [6–8]. Elevated levels of anxiety can lead to physiologic changes including

Table 1 Recommendations for addressing common challenges in pediatric body MRI

Challenge	Recommended sequence	Sample parameters for 3T	Notes
Motion degradation of T2-weighted images	Non-Cartesian T2 sequence: (e.g., PROPELLER T2)	Slice thickness: 5 mm Interslice gap: 0 mm FOV: 24–36 cm TR/TE: 6,375/94 ms Imaging plane: axial	Improved image quality at the expense of slightly longer scan time
Motion degradation of T1-weighted images	Non-Cartesian T1 sequence (e.g., radial T1 GRE)	Slice thickness: 2–3 mm Interslice gap: 1–1.5 mm FOV: 24–36 cm TR/TE: 2.7/1.3 ms Imaging plane: axial	Improved image quality, but inability to perform dynamic post-contrast imaging given the longer acquisition time
Inadequate arterial-phase imaging	Steady-state free precession 3-D inflow inversion recovery	Slice thickness: 1.4 mm Interslice gap: 0.7 mm FOV: 24–36 cm TR/TE: 3.7/1.69 ms Imaging plane: axial or coronal	No need for breath-hold (respiratory-gated acquisition). Best image quality with consistent breathing rate
Inability to administer intravenous contrast agent	Diffusion-weighted imaging	Slice thickness: 5 mm Interslice gap: 0 mm FOV: 34–36 cm TR/TE: 4,100/70 ms Imaging plane: axial	May be obtained with free breathing or respiratory gating. B values 0–800 mm/s^2
Small anatomical structures	3-D T2-weighted imaging	Slice thickness: 1.4 mm Interslice gap: 0.7 mm FOV: 24–36 cm TR/TE: 3,748/65 ms Imaging plane: coronal	No need for breath-hold (respiratory-gated acquisition). Best image quality with consistent breathing rate. Scan times longer than 2-D sequences (approximately 5 min total scan time)

FOV field of view, *GRE* gradient recall echo, *PROPELLER* periodically rotated overlapping parallel lines with enhanced reconstruction, *TE* echo time, *TR* repetition time

increased respiratory rates and muscle tension [9]. It is therefore not unexpected to have some degree of motion, even in the most cooperative children. This can lead to significant image degradation from motion artifacts, especially in children 6–10 years of age, for whom a non-sedated MRI study is often considered. This necessitates robust T1- and T2-weighted MRI pulse sequences that are motion-resistant. To help mitigate motion degradation, it is important to optimize MRI protocols, including making the appropriate adjustments to number of signal averages, breath-hold length, and use of respiratory gating [10]. Recent technical advances have led to improved image quality.

T1-weighted imaging

T1-weighted imaging is critical in characterizing lesions, assessing fat and blood products, and evaluating bone marrow. At most centers, conventional Cartesian T1-weighted sequences are used in standard pediatric abdomino-pelvic protocols. Yet traditional turbo or fast spin-echo (TSE/FSE) T1-weighted sequences are subject to long scan times and can be easily degraded by motion (Fig. 1). The advent of non-Cartesian sequences such as PROPELLER (periodically rotated overlapping parallel lines with enhanced reconstruction; GE Healthcare, Waukesha, WI), BLADE (Siemens Healthcare, Erlangen, Germany) and MultiVane (Philips Healthcare, Best, The Netherlands) using a radial sampling method with rotating blades of multiple phase-encoded lines and oversampling of the center of the k-space, and these features have helped to correct motion artifacts to improve resolution. Scan times, however, remain long with these techniques.

TI-weighted gradient recalled echo (GRE) sequences offer an alternative to standard TSE/FSE sequences and can be obtained more quickly, though with lower signal-to-noise ratio

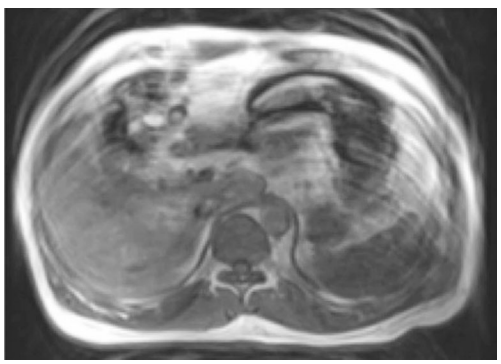

Fig. 1 Imaging challenge: breath-holding in a 7-year-old boy. Axial T1-W gradient recall echo in-phase MR image demonstrates marked respiratory motion degradation

(SNR). Respiratory-navigated versions of this sequence are available, such as respiratory-navigated LAVA (liver acquisition with volume acquisition; GE Healthcare; Fig. 2) [11]. This sequence aids in reducing respiratory motion and allows for increase in overall signal, though gross patient body motion remains an issue.

Another clinically available sequence to help reduce motion artifacts is the radial non-Cartesian T1-weighted gradient recalled echo sequence known as VIBE (volumetric interpolated breath-hold examination, also known as Star-VIBE by Siemens Healthcare) [12–14]. This sequence provides several advantages over conventional 3-D T1-weighted GRE imaging, including free breathing, motion robustness and high spatial resolution [15]. In Star-VIBE, data are acquired in the central region of k-space [16]. Radial imaging spokes are acquired along the k_x and k_y planes while conventional sampling occurs along the k_z plane, resulting in a complete 3-D sampling often referred to as the "stack of stars" [15].

Motion artifacts in conventional Cartesian k-space trajectories result in ghosting artifacts in the phase-encoding direction. However for radial k-space trajectories, the motion artifacts are effectively spread throughout the entire field of view (FOV). Artifacts from motion become less noticeable and have minimal impact on quality. This sequence allows one to scan for a longer period of time and is much less sensitive to motion, making it ideal for use in pediatrics. Both Chandarana et al. [12] and Roque et al. [17] have shown that there is significantly higher image quality in using radial-VIBE sequences over conventional VIBE in evaluating children. Chandarana and colleagues [12] described increased conspicuity and detection of lesions when comparing radial VIBE to equivalent non-radial sequences. The main disadvantage of Star-VIBE is that it can't be used for performing dynamic contrast-enhanced imaging and thus it is limited to imaging in the equilibrium phase after intravenous contrast administration. Therefore it is ideal for children who cannot breath-hold and in situations where respiratory gating becomes inadequate (Fig. 3). Further research is required to overcome the disadvantages of radial imaging. Other sequences such as GRASP (golden angle radial sparse parallel MR imaging) and KWIK (k-space weighted image contrast) are under investigation but are not clinically available [12, 15].

Fig. 2 T1-W LAVA sequence in a 12-year-old girl with elevated lipase and chronic abdominal pain. Coronal respiratory-navigated FSPGR T1 with fat saturation (LAVA Flex) sequence demonstrates no significant motion artifact and homogeneous fat saturation. The mucosa of the small and large bowel is clearly seen. Note the swirl of material within the urinary bladder (*arrow*). *FSPGR* fast spoiled gradient recalled acquisition in the steady state, *LAVA* liver acquisition with volume acceleration

An additional consideration in pediatric abdomino-pelvic T1-weighted imaging is magnetic field inhomogeneity, which is more pronounced in the abdomen and pelvis than other areas of the body, particularly at 3T. Smaller patient body sizes further manifest the effect of this inhomogeneity because they are often farther from the isocenter of the magnet, and as such make homogeneous fat saturation with T1-weighted imaging challenging. While use of padding or cushions to move these small patients closer to the isocenter of the magnet can lessen the effect, incorporation of T1 GRE Dixon fat-and-water-separation techniques also provides more consistent homogeneous fat saturation (Fig. 4) and can be performed with breath-hold or respiratory navigation [11, 18]. These techniques allows for consistent, high-quality T1-weighted assessment of pediatric abdominal pathology.

T2-weighted imaging

T2-weighted imaging is useful for characterizing lesions, detecting fluid-containing structures, and assessing blood products. Similar to T1-weighted imaging, standard Cartesian-based T2-weighted imaging can be performed using respiratory gating [19] or with breath-holds [20–22].

Also similar to T1-weighted imaging, non-Cartesian methods are available for T2-weighted assessment in the body, such as PROPELLER, BLADE and MultiVane [23]. These techniques allow for high-quality assessment of abdominal and pelvic viscera (Fig. 5). Non-Cartesian T2-weighted images have demonstrated equivalent to superior performance in image quality and lesion detection in comparison to standard TSE/FSE methods [24–26]. The main disadvantage with this technique is slightly longer scan times (approximately 3–5 min longer on average in the author's experience). Streak artifacts can be noted with this technique, particularly in cases of patient motion, and are most pronounced at the diaphragms

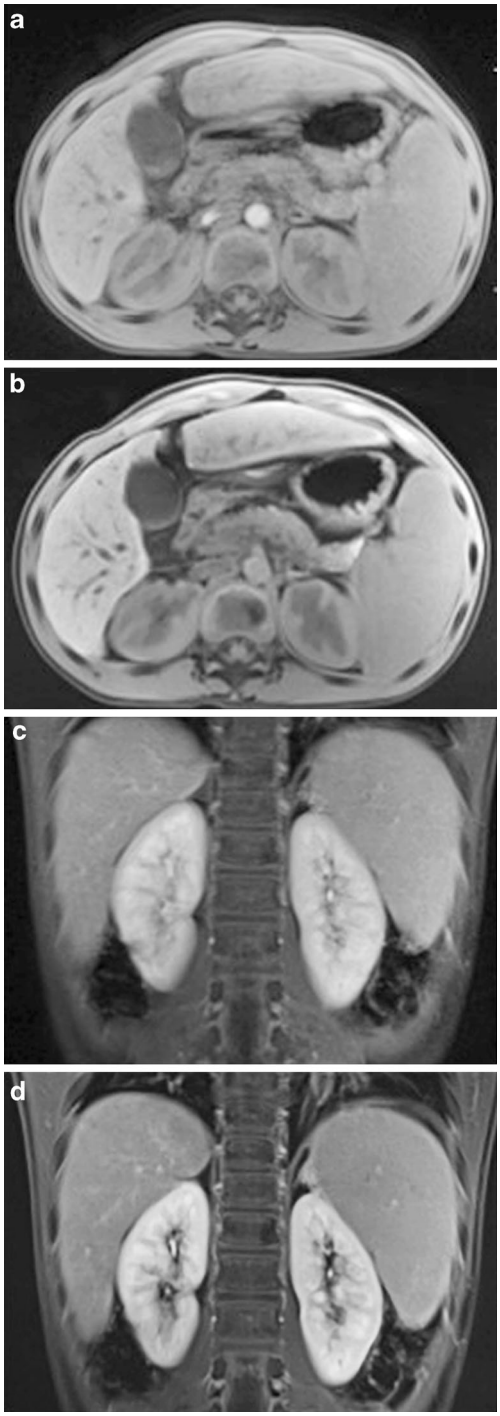

Fig. 3 T1-W VIBE imaging in a 7-year-old boy with embryonal rhabdomyosarcoma who had routine surveillance imaging. This study was performed without sedation but with the assistance of a child life specialist. **a** Axial Cartesian T1 VIBE with fat suppression image obtained with a 20-s breath-hold shows artifact from breathing at the interfaces of the solid organs, particularly the liver. **b** Axial non-Cartesian Star-VIBE with fat suppression image obtained during free-breathing as a continuous acquisition over 2 min. In contrast to (**a**), the Star-VIBE is motion robust, with clean margins at the edges of the liver, spleen, pancreas and kidneys. **c**, **d** Post-contrast coronal T1-W VIBE (**c**) and Star-VIBE (**d**) side-by-side show the superior resolution and clarity of the structures with Star-VIBE. *VIBE* volume-interpolated breath-hold examination

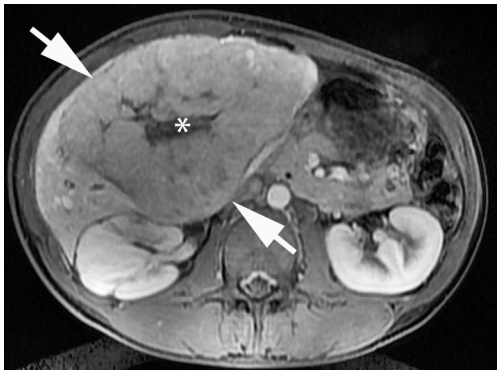

Fig. 4 T1-W LAVA imaging in a 16-year-old boy with known fibrolamellar hepatocellular carcinoma. MR was obtained to assess for metastatic lesions. Axial FSPGR (fast spoiled gradient recalled acquisition in the steady state, LAVA Flex) obtained in late arterial phase at 3 tesla demonstrates a large hepatic mass (*arrows*) with a non-enhancing central scar (*asterisk*). Note the overall homogeneous fat saturation throughout the image. *LAVA* liver acquisition with volume acceleration

and in the bowel. The considerations between overall image quality and the compromise of increased scan time and potential streaking artifact must be carefully weighed (Fig. 6).

Non-contrast vascular imaging

When assessing arteries, optimal timing of arterial-phase imaging can be technically challenging because of issues with breath-holding, smaller arterial diameters, and low volumes of contrast agent in small children (given weight-based dosing). Therefore robust non-contrast methods of vascular assessment as well as non-contrast means of evaluating inflammation and characterizing lesions are highly valuable in pediatric MRI. Two such methods are 3-D steady-state free precession and diffusion-weighted imaging.

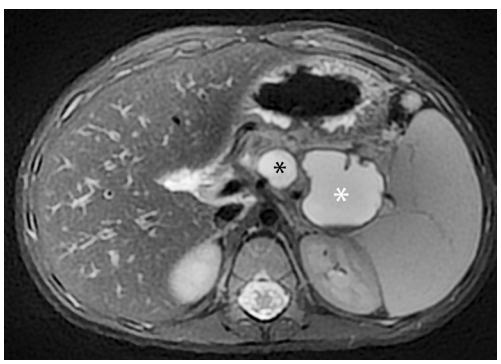

Fig. 5 T2-W PROPELLER in a 4-year-old boy with cystic mass seen on ultrasound. Axial PROPELLER T2-W fat-saturated image obtained at 3 tesla demonstrates a large pseudocyst in the pancreatic tail (*white asterisk*) and a smaller pseudocyst in the pancreatic body (*black asterisk*) in this boy with familial pancreatitis. *PROPELLER* periodically rotated overlapping parallel lines with enhanced reconstruction

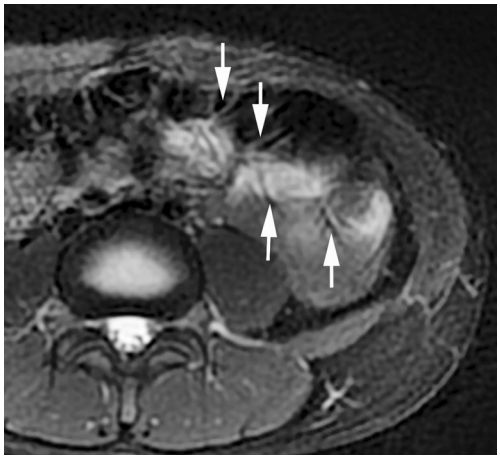

Fig. 6 T2-W PROPELLER in a 13-year-old girl with family history of Crohn disease, presenting with abdominal pain and nausea. Axial PROPELLER T2-W fat-saturated image obtained at 3 tesla demonstrates streak artifact (*arrows*), a known artifact seen in radial blade-type imaging. This artifact is particularly prominent in moving structures such as peristalsing bowel. *PROPELLER* periodically rotated overlapping parallel lines with enhanced reconstruction

3-D steady-state free precession

An additional challenge that must be considered in children is the use of intravenous (IV) contrast agent. A number of factors can make IV contrast-enhanced imaging difficult in pediatric patients. Children have smaller vessels, making intravenous access more challenging. Furthermore, with weight-based dosing of gadolinium-based contrast agents, smaller children require as little as 1 mL or less of intravenous contrast for imaging. This leads to technical challenges in achieving optimal timing for arterial-phase imaging. Early work with non-contrast-enhanced MR angiographic sequences included phase-contrast and time-of-flight imaging [27, 28]; however these sequences are of overall lower resolution when used in the abdomen and pelvis, with limited utility in performing high-resolution post-processing. Furthermore, these sequences are more susceptible to patient motion and magnetic field inhomogeneity [27, 28].

The use of alternative methods to achieve higher-resolution three-dimensional (3-D) non-contrast MR angiographic images using balanced steady-state free precession (b-SSFP) were described by Miyazaki et al. [29] as early as 2008. More recent clinical implementation of the following sequences has allowed for highresolution non-contrast 3-D MR angiographic imaging to be obtained in the abdomen and pelvis: inhance inflow inversion recovery (IFIR) by GE Healthcare; b-TRANCE (triggered angiography noncontrast-enhanced) by Philips Healthcare; NATIVE (noncontrast MR angiography of arteries and veins); TrueFISP (true fast imaging with steady-state precession) by Siemens Healthcare. The sequence is obtained with respiratory gating (avoiding the need for breath-holding) and can be post-processed to create high-resolution maximum-intensity projection (MIP) and 3-D images (Fig. 7). Scan times are in the order of 3 min or less in total. Recent studies in adults have shown equivalent diagnostic capability of this sequence in comparison to CT angiography and contrast-enhanced MR angiography [30, 31]. This sequence is limited by inconsistent breathing rates and patterns, and volumes of inspiration.

Diffusion-weighted imaging (DWI)

Diffusion-weighted imaging (DWI) takes advantage of the differences in Brownian motion of water molecules within various tissues [32]. Areas of high cellularity demonstrate restricted diffusion and, therefore, hyperintense signal. The degree of restricted diffusion is in inverse proportion to the cellularity and membrane integrity, and it can be measured by the apparent diffusion coefficient (ADC) [32]. DWI has been shown to be a viable alternative to IV contrast enhancement for characterizing inflammation (in cases of inflammatory bowel disease) and detecting lesions (in the solid organs) [33–36]. In body imaging, b values in the range of 600–1,000 s/mm^2 are typically used for assessing inflammation and characterizing lesions (Fig. 8). The addition of lower b values (b=20–100 mm/s^2) can aid both in detecting lesions and in calculating perfusional components

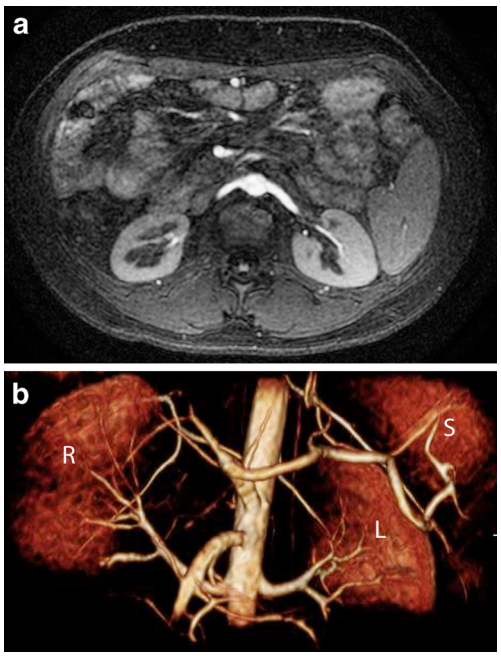

Fig. 7 Three-dimensional angiography in a 17-year-old girl with a history of hepatitis C being evaluated for liver transplant. **a** Axial source MR image of inflow inversion recovery 3-D steady-state free precession non-contrast MR angiography sequence demonstrates hyperintense signal within the aorta, with suppressed background signal in the remaining tissues. **b** Coronal 3-D volume rendering generated on a separate workstation from the same source data demonstrates the major arterial structures of the abdomen. Spleen (*S*), right kidney (*R*) and left kidney (*L*) are noted with major supplying arteries

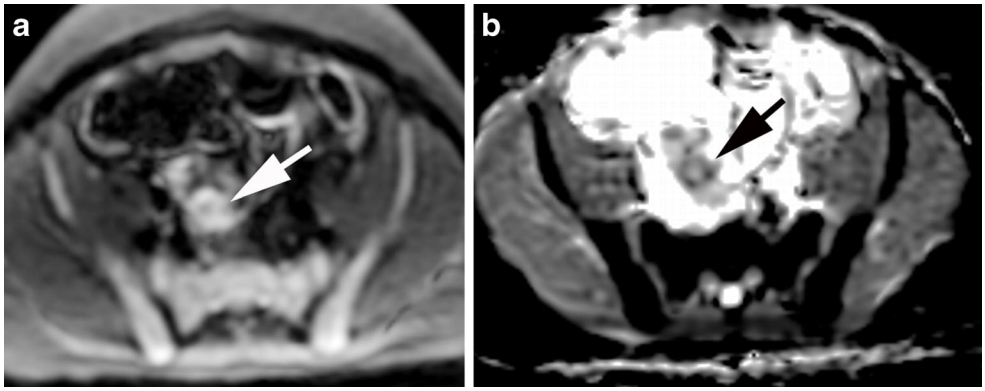

Fig. 8 Diffusion-weighted imaging in a 14-year-old boy with intermittent severe abdominal pain, lower abdominal pain on exam, and concern for constipation. The boy was referred for MR enterography. **a** Unexpectedly, diffusion-weighted imaging demonstrates hyperintense signal of the appendix. **b** Corresponding apparent diffusion coefficient map shows corresponding low signal, compatible with restricted diffusion in this case of acute appendicitis

of tissue diffusion when performing bi-exponential DWI calculations using intravoxel incoherent motion (IVIM) [37, 38]. It must be considered, however, that each added b value comes at the expense of additional scan time. DWI can be performed using a free-breathing technique such as diffusion-weighted imaging with background body signal suppression (DWIBS), which typically uses high b values (800–1,000 s/mm^2), non-Cartesian radial technique, or a respiratory gated multi-b value approach [39–42]. These techniques allow for higher-signal imaging and thinner slices to be obtained. In cases where IV access cannot be obtained or renal function is not adequate to perform IV contrast-enhanced imaging, DWI offers a valuable alternative.

High-resolution post-contrast imaging

In order to achieve optimal dynamic contrast-enhanced MR images there are tradeoffs in both temporal and spatial resolution. Having robust T1-weighted sequences is an important precursor to further acquiring high-quality post-contrast images.

There are a few important steps to be taken just prior to administering IV contrast to help ensure diagnostic-quality post-contrast T1 sequences. It is important for the child to be adequately sedated or anesthetized just prior to the injection of a gadolinium chelate to avoid the child awakening during the dynamic contrast-enhanced portion. In some cases of liver masses, an MR exam under anesthesia with intubation allows for respiratory suspension to yield better-quality dynamic contrast-enhanced MR imaging sequences with minimal motion artifact from breathing. Proper breath-hold techniques should be practiced either just before the contrast injection or in advance of the MRI examination on a mock MRI scanner or with child life experts [43]. These tactics are valuable and helpful to ensure high-quality diagnostic studies.

Post-contrast imaging at 3T can be challenging because of the greater number of susceptibility artifacts encountered over imaging at 1.5T. Although in principle one would expect a two-fold increase in SNR for a higher-field-strength magnet, the actual SNR is less because of the longer T1 relaxation times at 3T. Other important factors to obtain high-quality imaging at 3T are rapid acquisition, strong T1-weighting, high SNR and contrast-to-noise ratio. Strong T1-weighting can be achieved by using the shortest repetition time (TR) possible and adjusting the flip angle, but care needs to be taken not to exceed the specific absorption rate limits [44]. In addition, shorter echo time (TE) values help to reduce susceptibility artifact and may improve fat suppression [44]. However, there are tradeoffs in using short TE and TR values because this can result in using higher receiver bandwidth values, which can in turn reduce overall SNR [44].

In addition to the conventional dynamic post-contrast T1-weighted sequences, there are a few new post-contrast T1-weighted 3-D spoiled gradient echo imaging techniques worth discussing. These include CAIPIRINHA (controlled aliasing parallel imaging results in higher acceleration; Siemens) and DISCO (differential sub-sampling with Cartesian ordering; GE Healthcare, Waukesha, WI). CAIPIRINHA enables one to acquire a shorter breath-hold scan over conventional 3-D T1-weighted GRE sequence using higher acceleration factors. A detailed discussion of the physics behind these new techniques is beyond the scope of this paper but has been published elsewhere [45, 46]. Although published data show that there is no significant difference in quality of the images between CAIPIRINHA and traditional 3-D T1-weighted GRE (VIBE) [47], in practice this could be viewed differently. In fact, image quality can be improved if the breath-hold is more practical and convenient for a pediatric patient; the new technique requires 16 s for breath-hold versus 18–22 s for traditional volumetric T1 acquisition (Fig. 9). DISCO is an alternative method of dynamic contrast-enhanced MRI, providing both high spatial and temporal resolution. Within one 15-s

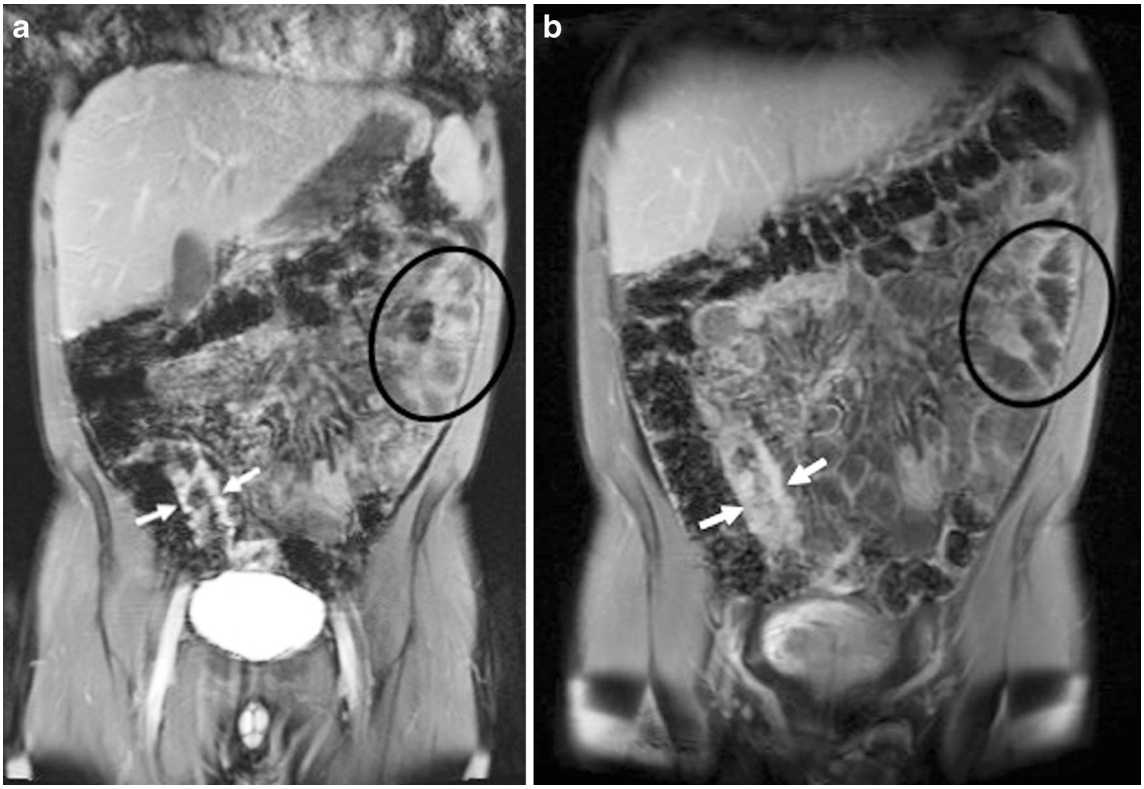

Fig. 9 CAIPIRINHA sequence in a 14-year-old boy with Crohn disease and terminal ileitis. He had MR enterography at two separate time points on a 3-T magnet. **a** The first MR examination was a conventional coronal post-contrast dynamic T1-weighted VIBE with fat suppression, performed with a 12-s breath-hold. **b** The follow-up exam was performed with the newer CAIPIRINHA coronal post-contrast dynamic T1-weighted VIBE, with an 8.1-s breath-hold. The shorter breath-hold results in significantly improved resolution, with less artifact from breathing and a clearer depiction of the TI inflammation (*arrows*). Note the well-defined evaluation of the bowel wall of the jejunal loops in the left upper quadrant (*circle*). *CAIPIRINHA* controlled aliasing parallel imaging results in higher acceleration, *VIBE* volume-interpolated breath-hold examination

breath hold, multiple phases can be obtained. DISCO achieves this by using a dual-echo spoiled gradient recalled echo (SPGR) sequence in combination with pseudo-random variable density k-space segmentation and a view-sharing reconstruction (Fig. 10). A Dixon reconstruction algorithm is used to achieve fat and water separation (Fig. 11) [48].

High-resolution T2-W imaging

High-resolution T2-weighted FSE/TSE sequences, both 2-D and 3-D, are important in the evaluation of the pediatric abdomen. In particular, 3-D T2-weighted images complement 2-D T2-weighted sequences, which are often subject to lower spatial resolution and low SNR [49]. The other major advantage of 3-D T2 data is their utility in reconstructing any plane using surface-shaded renderings, volume renderings or maximum-intensity projections (MIPs).

In contrast to earlier versions, isotropic 3-D T2-weighted SPACE (sampling perfection with application optimized contrasts using different flip-angle evolutions; Siemens) is a variation of 3-D TSE sequence with a flip angle of less than 180°, which affords a larger number of refocusing pulses per repetition time [50]. Similar 3-D T2-weighted sequences exist with other vendors (CUBE by GE Healthcare, or volume isotropic turbo spin-echo acquisition [VISTA] by Philips Healthcare). This sequence is advantageous because it provides overall excellent T2 signal and higher, especially at 3T. Prior publications have shown how 3-D T2 SPACE yields superior quality imaging to traditional TSE T2-weighted imaging and performs better at 3T versus 1.5T [50, 51]. The 3-D T2-weighted volumetric acquisition acquires thin (1-mm) contiguous slices, which takes several minutes even with parallel imaging and requires use of respiratory triggering or navigator gating when applying it in children.

The 3-D T2-weighted FSE sequence is a valuable part of the MR urography and MR cholangiopancreatography protocols. When imaging a dilated upper urinary tract, whether in a single system or duplex, 3-D reconstructions clearly delineate the course and insertion of the ureter [52]. This is particularly important for identifying ectopic ureteral insertions, which are challenging for urologists to see at cystoscopy and therefore can guide management [22]. The 3-D reformats are also helpful to show the course of insertion of the ureters associated with complex congenital anomalies such as cross-fused ectopia or

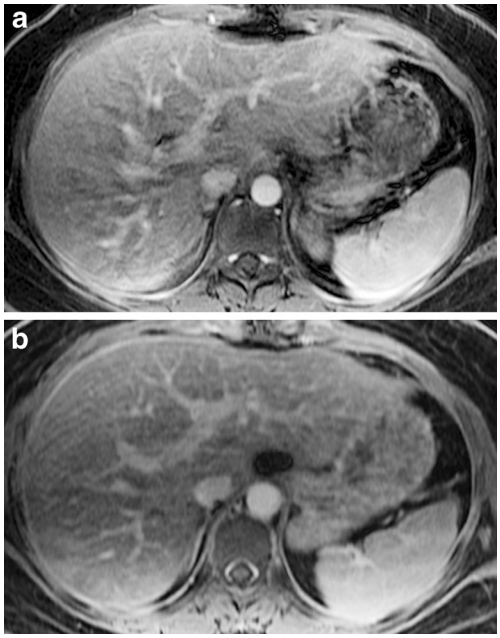

Fig. 10 DISCO imaging in a 22-year-old woman post liver transplant, with history of persistently elevated transaminases. **a** The woman had difficulty suspending respiration during the 15-s breath-hold 3-D T1-W SPGR fat-saturated (LAVA Flex) axial post-contrast sequence, resulting in motion degradation. Following the dynamic post-contrast series, a multiphasic respiratory-navigated 3-D T1-W SPGR (DISCO) sequence was obtained, for a total scan time of 1 min 5 s. **b** A single phase of the five phases obtained within this 1 min 5 s period demonstrates decreased motion blurring, particularly in the hepatic vasculature. *DISCO* differential sub-sampling with Cartesian ordering, *SPGR* spoiled gradient recalled echo

horseshoe kidney (Fig. 12) [22, 49]. Similar to urological work, one can use the 3-D T2-W FSE MR images to create reconstructions of congenital abnormalities of the bile and pancreatic ducts. This can better depict an entire lesion in one image or identify more clearly the pancreaticobiliary junction and serve as a potential roadmap for surgery versus medical management (Figs. 13, 14 and 15).

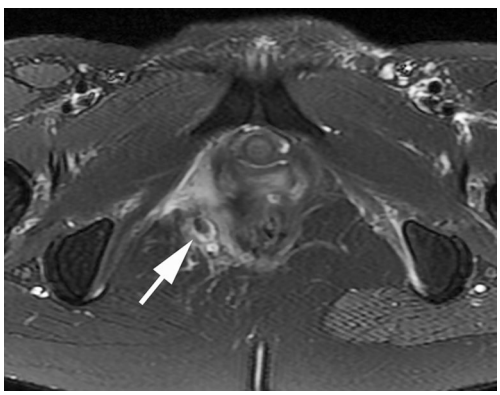

Fig. 11 Dixon technique in a 15-year-old with with history of colectomy for ulcerative colitis. She presented with abdominal mass, pain and fever. High-resolution T2-weighted fast spin-echo axial MR image with Dixon technique demonstrates a fistula in the left ischiorectal fossa (*arrow*) in the girl, who was later found to have Crohn disease

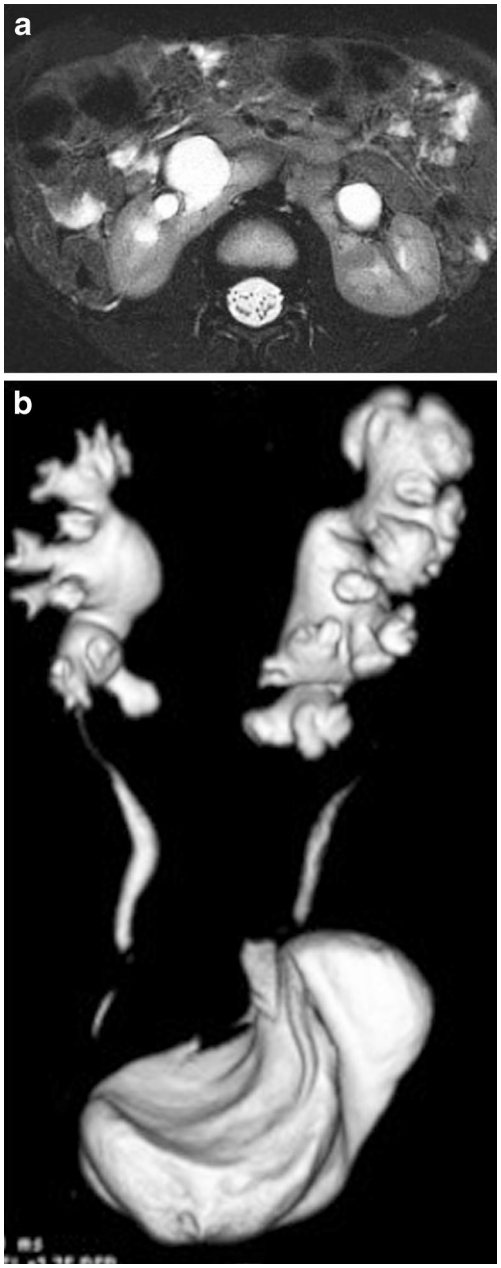

Fig. 12 SPACE in a 2-year-old boy with a horseshoe kidney and ureteropelvic junction (UPJ) obstruction in the right-side renal moiety. MR urography was performed to identify the course and insertion of the right moiety ureter. **a** Axial high-resolution T2-weighted MR sequence with fat suppression shows the horseshoe configuration with dilatation of the right-side moiety and UPJ. **b** A posterior projection of a shaded surface display created from a 3-D T2-weighted SPACE volumetric acquisition shows the horseshoe configuration with dilated collecting system and the ureters from each moiety inserting orthotopically into the bladder. *SPACE* sampling perfection with application optimized contrasts using different flip-angle evolutions

Hepatic iron quantification

Liver iron overload can occur in conditions such as primary hemochromatosis, transfusional hemosiderosis in children with sickle cell hemoglobinopathies, thalassemia,

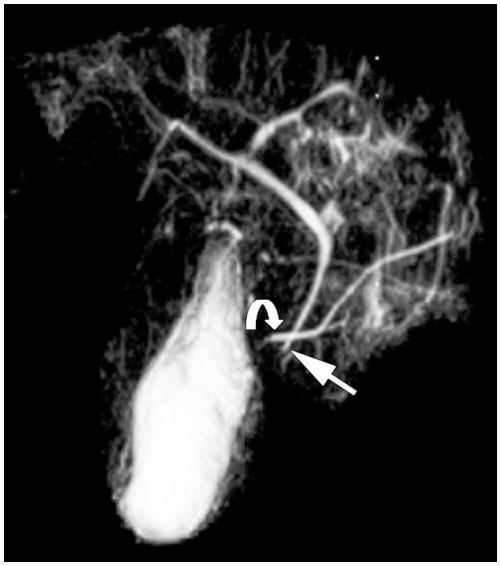

Fig. 13 Three-dimensional T2-W MR in a 6-year-old boy with recurrent pancreatitis diagnosed with pancreas divisum. A shaded surface display created from a 3-D T2-weighted dataset shows a classic pancreas divisum, where the common bile duct is draining into the major papilla (*straight arrow*) whereas the pancreatic duct is draining more superiorly into the minor papilla (*curved arrow*)

and in chronic liver diseases. Severe iron overload can lead to cellular damage and diminished organ function in the liver and heart. Thus methods to accurately quantify liver iron deposition are important to allow for appropriate clinical management. While non-targeted percutaneous liver biopsy and estimation of liver iron concentration (LIC) is the gold standard method of liver iron quantification, biopsy does have limitations because of its invasiveness and sampling variability [53]. MRI is a very

Fig. 14 Three-dimensional MR cholangiopancreatography in a 17-year-old girl with choledochal cyst. Volume-rendered image obtained from 3-D MR cholangiopancreatography source data demonstrates fusiform dilation of the common bile duct (*C*) and central intrahepatic ducts compatible with a type IV choledochal cyst. Gallbladder (*G*) abuts the dilated common bile duct

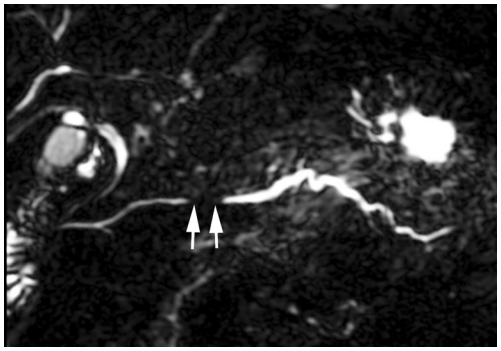

Fig. 15 Maximum-intensity projection MR imaging in a 12-year-old boy with recurrent pancreatitis. Coronal curved planar image of the main pancreatic (Wirsung) duct demonstrates a focal stricture in the mid-pancreatic body (*arrows*)

commonly used noninvasive method of liver iron quantification because of its availability and lack of ionizing radiation. The MRI methods include signal intensity ratio techniques using T2- or T2*-weighted images, R2 (1/T2) and R2* (1/T2*) relaxometry techniques, and MR susceptometry.

The most popular of the signal intensity ratio (SIR) methods is that of Gandon and colleagues [54], which uses a combination of five breath-hold GRE sequences with different T1, proton density, T2 and T2* weighting. Using their specific parameters, LIC can be estimated. The Gandon method has several limitations, with its accuracy being affected by macroscopic field inhomogeneities and the variability of coil sensitivity profiles.

The R2 relaxometry technique uses a series of single spin echoes (SSE), each acquired after a separate excitation, or by using a train of spin echoes following a single excitation using a Carr–Purcell–Meiboom–Gill sequence [55]. The echo times used typically range from <5 ms to 15–30 ms. R2 can be estimated by plotting the decay of signal intensity values with TE as a mono-exponential or bi-exponential decay. The main limitation of the R2 relaxometry method is the long acquisition time required for R2 mapping by using SSE image sequences. The St. Pierre method is the most popular R2 relaxometry technique based on the non-linear relationship between R2 and LIC [56]. This method was approved by the U.S. Food & Drug Administration in 2005 and is commercially available as FerriScan® (ResonanceHeath, Claremont, WA, Australia). FerriScan® is robust and well validated. The limitations, however, include the cost per study, time of acquisition (10–20 min) and possibly the report turnover time of approximately 2 business days.

R2* relaxometry, based on gradient echo acquisition (to measure T2*) has the potential to overcome some of the limitations of the R2-based techniques because it provides full liver coverage without motion artifacts in a single breath-hold [53]. The T2* estimation method has

become the most common quantification method. A 1.5-T MR scanner is preferred to 3T or other field strengths, partly because of the higher availability of 1.5T, and most of the literature on calibration of liver iron concentration is based on T2* values at 1.5T. There is also increased dephasing from T2* effect and rapid loss of signal that happens with 3T as compared to 1.5T field strength. T2* can be obtained by performing multiple gradient echo sequences (2-D or 3-D spoiled gradient echo) with different TE values from 1 ms to 20 ms with a fixed TR. Prescanning should not be performed between sequences because the transmit-and-receive gains could change [57]. It may be necessary to use a small frequency matrix (192 or 224), fractional echo sampling, and high receiver bandwidth (>100 kHz) to achieve the appropriate echo time combination [53, 57].

A region of interest (ROI) can be placed on the same location in the liver for the images obtained at different TE values. The mean signal intensity value obtained can be plotted to exhibit an exponential decay. When the natural logarithmic value of the ROI is plotted against TE values (in milliseconds), there is a linear drop in signal with gradual flattening of the slope because of noise. The inverse of the slope of this plot (excluding the signal from the background noise and ignoring the negative sign) is the T2* value (in milliseconds). T2* value multiplied by 1,000 gives R2* (in Hertz). R2* value can be used to calculate the iron content in the liver. One of the more well-known and accepted methods for estimating LIC (in mg/g dry liver weight) is that by Wood [58], Hernando et al. [53] and Tran et al. [57], using the following equation: $LIC=0.0254\times R2^* +0.202$

The above equation has been validated for 1.5-T magnetic field strength using imaging parameters and image reconstruction as described by Wood [58]. It has, however, been shown that R2* at 3T magnetic field strength is two times the value obtained at 1.5T and therefore this can be used to also estimate LIC on 3-T MR scanners. Nevertheless, because of the 2-times faster loss of signal at 3T as compared to 1.5T, higher liver iron concentration cannot be evaluated accurately, which is even an issue at 1.5-T field strength for extreme iron overload. Ultrashort TE techniques can be helpful to overcome this limitation [53, 59].

To exclude ROI signal values resulting from background noise, only the ROI signal values in the steepest linear portion are used for calculation of R2* value. Hepatic fat can confound the estimation of LIC, but it is usually not much of an issue in the pediatric population. A typical MR protocol includes T1 in-phase and opposed-phase images to show whether there is any significant hepatic fat deposition. Using consistent image acquisition protocols and T2* quantification methods, good inter-center and intra-center reproducibility of results can be achieved.

Summary

In this review, we have highlighted a number of techniques that have recently been developed to address many of the challenges encountered in pediatric abdomino-pelvic imaging. These newer techniques can help pediatric radiologists to overcome some of the challenges in clinical body MR imaging.

Compliance with ethical standards

Conflicts of interest None

References

1. Parker MW, Shah SS, Hall M et al (2015) Computed tomography and shifts to alternate imaging modalities in hospitalized children. Pediatrics 136:e573–e581
2. Jung D, Denna J, John W et al (2016) Cardiac magnetic resonance imaging can be performed without the use of anesthesia in patients 7–10 years of age with child life support and MRI video goggles. J Cardiovasc Magn Reson 18:O120
3. Durand DJ, Mollie Y, Paul N et al (2015) Mandatory child life consultation and its impact on pediatric MRI workflow in an academic medical center. J Am Coll Radiol 12:594–598
4. Harned RK 2nd, Strain JD (2001) MRI-compatible audio/visual system: impact on pediatric sedation. Pediatr Radiol 31:247–250
5. Courtier J, Cardenas A, Tan C et al (2015) Non-anesthesia MR enterography in very young children — feasibility, technique and performance. J Pediatr Gastroenterol Nutr. doi:10.1097/MPG.0000000000000712
6. Greene DJ, Black KJ, Schlaggar BL (2016) Considerations for MRI study design and implementation in pediatric and clinical populations. Dev Cogn Neurosci 18:101–112
7. Poldrack RA, Paré-Blagoev EJ, Grant PE (2002) Pediatric functional magnetic resonance imaging: progress and challenges. Top Magn Reson Imaging 13:61–70
8. Kotsoni E, Eleni K, Dana B et al (2006) Special considerations for functional magnetic resonance imaging of pediatric populations. J Magn Reson Imaging 23:877–886
9. Drevets WC, Videen TQ, MacLeod AK et al (1992) PET images of blood flow changes during anxiety: correction. Science 256:1696
10. Chavhan GB, Babyn PS, Vasanawala SS (2013) Abdominal MR imaging in children: motion compensation, sequence optimization, and protocol organization. Radiographics 33:703–719
11. Vasanawala SS, Iwadate Y, Church DG et al (2010) Navigated abdominal T1-W MRI permits free-breathing image acquisition with less motion artifact. Pediatr Radiol 40:340–344
12. Chandarana H, Hersh C, Block KT et al (2013) Free-breathing contrast-enhanced T1-weighted gradient-echo imaging with radial k-space sampling for paediatric abdominopelvic MRI. Eur Radiol 24:320–326
13. Shin HJ, Kim M-J, Lee M-J et al (2016) Comparison of image quality between conventional VIBE and radial VIBE in free-breathing paediatric abdominal MRI. Clin Radiol 71:1044–1049
14. Fujinaga Y, Yasunari F, Ayumi O et al (2014) Radial volumetric imaging breath-hold examination (VIBE) with k-space weighted image contrast (KWIC) for dynamic gadoxetic acid (Gd-EOB-

DTPA)-enhanced MRI of the liver: advantages over Cartesian VIBE in the arterial phase. Eur Radiol 24:1290–1299
15. Kierans A, Parikh N, Chandarana H (2015) Recent advances in MR hardware and software. Radiol Clin N Am 53:599–610
16. Fujinaga Y, Yasunari F, Yoshihiro K et al (2015) Advantages of radial volumetric breath-hold examination (VIBE) with k-space weighted image contrast reconstruction (KWIC) over Cartesian VIBE in liver imaging of volunteers simulating inadequate or no breath-holding ability. Eur Radiol 26:2790–2797
17. Roque A, Andreia R, Miguel R et al (2014) Post-contrast T1-weighted sequences in pediatric abdominal imaging: comparative analysis of three different sequences and imaging approach. Pediatr Radiol 44:1258–1265
18. Li XH, Jiang Z, Zhang XM et al (2013) Abdominal MRI at 3.0 T: LAVA-Flex compared with conventional fat suppression T1-weighted images. J Magn Reson Imaging 40:58–66
19. Taylor AM, Jhooti P, Wiesmann F et al (1997) MR navigator-echo monitoring of temporal changes in diaphragm position: implications for MR coronary angiography. J Magn Reson Imaging 7: 629–636
20. Augui J, Vignaux O, Argaud C et al (2002) Liver: T2-weighted MR imaging with breath-hold fast-recovery optimized fast spin-echo compared with breath-hold half-Fourier and non-breath-hold respiratory-triggered fast spin-echo pulse sequences. Radiology 223:853–859
21. Reinig JW (1995) Breath-hold fast spin-echo MR imaging of the liver: a technique for high-quality T2-weighted images. Radiology 194:303–304
22. Adeb M, Darge K, Dillman JR et al (2013) Magnetic resonance urography in evaluation of duplicated renal collecting systems. Magn Reson Imaging Clin N Am 21:717–730
23. Pipe JG (1999) Motion correction with PROPELLER MRI: application to head motion and free-breathing cardiac imaging. Magn Reson Med 42:963–969
24. Lane BF, Vandermeer FQ, Oz RC et al (2011) Comparison of sagittal T2-weighted BLADE and fast spin-echo MRI of the female pelvis for motion artifact and lesion detection. AJR Am J Roentgenol 197:W307–W313
25. Rosenkrantz AB, Mannelli L, Mossa D et al (2011) Breath-hold T2-weighted MRI of the liver at 3 T using the BLADE technique: impact upon image quality and lesion detection. Clin Radiol 66: 426–433
26. Haneder S, Dinter D, Gutfleisch A et al (2011) Image quality of T2W-TSE of the abdomen and pelvis with Cartesian or BLADE-type k-space sampling: a retrospective interindividual comparison study. Eur J Radiol 79:177–182
27. Maki JH, Wilson GJ, Eubank WB et al (2007) Steady-state free precession MRA of the renal arteries: breath-hold and navigator-gated techniques vs CE-MRA. J Magn Reson Imaging 26:966–973
28. Silverman JM, Friedman ML, Van Allan RJ (1996) Detection of main renal artery stenosis using phase-contrast cine MR angiography. AJR Am J Roentgenol 166:1131–1137
29. Miyazaki M, Mitsue M, Lee VS (2008) Nonenhanced MR angiography 1. Radiology 248:20–43
30. Glockner JF, Naoki T, Akira K et al (2010) Non-contrast renal artery MRA using an inflow inversion recovery steady state free precession technique (Inhance): comparison with 3D contrast-enhanced MRA. J Magn Reson Imaging 31:1411–1418
31. Xu J-L, Shi D-P, Li Y-L et al (2011) Non-enhanced MR angiography of renal artery using inflow-sensitive inversion recovery pulse sequence: a prospective comparison with enhanced CT angiography. Eur J Radiol 80:e57–e63
32. Chavhan GB, Zehour A, Babyn PS (2014) Diffusion-weighted imaging in pediatric body MR imaging: principles, technique, and emerging applications. Radiographics 34:E73–E88
33. Fehniger J, Thomas S, Lengyel E et al (2016) A prospective study evaluating diffusion weighted magnetic resonance imaging (DW-MRI) in the detection of peritoneal carcinomatosis in suspected gynecologic malignancies. Gynecol Oncol 142: 169–175
34. Ream JM, Dillman JR, Jeremy A et al (2013) MRI diffusion-weighted imaging (DWI) in pediatric small bowel Crohn disease: correlation with MRI findings of active bowel wall inflammation. Pediatr Radiol 43:1077–1085
35. Neubauer H, Henning N, Thomas P et al (2012) Small-bowel MRI in children and young adults with Crohn disease: retrospective head-to-head comparison of contrast-enhanced and diffusion-weighted MRI. Pediatr Radiol 43:103–114
36. Shenoy-Bhangle AS, Katherine N, Thomas A et al (2015) Value of diffusion-weighted imaging when added to magnetic resonance enterographic evaluation of Crohn disease in children. Pediatr Radiol 46:34–42
37. Parikh T, Drew SJ, Lee VS et al (2008) Focal liver lesion detection and characterization with diffusion-weighted MR imaging: comparison with standard breath-hold T2-weighted imaging. Radiology 246:812–822
38. Koh D-M, Collins DJ, Orton MR (2011) Intravoxel incoherent motion in body diffusion-weighted MRI: reality and challenges. AJR Am J Roentgenol 196:1351–1361
39. Kachewar SG (2011) Using DWIBS MRI technique as an alternative to bone scan or PET scan for whole-body imaging in oncology patients. Acta Radiol 52:788
40. Li Z, Pipe JG, Lee C-Y et al (2011) X-PROP: a fast and robust diffusion-weighted PROPELLER technique. Magn Reson Med 66:341–347
41. Deng J, Miller FH, Salem R et al (2006) Multishot diffusion-weighted PROPELLER magnetic resonance imaging of the abdomen. Investig Radiol 41:769–775
42. Mürtz P, Petra M, Carsten K et al (2007) Diffusion-weighted whole-body MR imaging with background body signal suppression: a feasibility study at 3.0 tesla. Eur Radiol 17:3031–3037
43. Anupindi SA, Podberesky DJ, Towbin AJ et al (2015) Pediatric inflammatory bowel disease: imaging issues with targeted solutions. Abdom Imaging 40:975–992
44. Bhatti L, Hoang JK, Dale BM et al (2015) Advanced magnetic resonance techniques: 3 T. Radiol Clin N Am 53:441–455
45. Breuer FA, Blaimer M, Mueller MF et al (2006) Controlled aliasing in volumetric parallel imaging (2D CAIPIRINHA). Magn Reson Med 55:549–556
46. Yutzy SR, Seiberlich N, Duerk JL et al (2011) Improvements in multislice parallel imaging using radial CAIPIRINHA. Magn Reson Med 65:1630–1637
47. Morani AC, Vicens RA, Wei W et al (2015) CAIPIRINHA-VIBE and GRAPPA-VIBE for liver MRI at 1.5 T. J Comput Assist Tomogr 39:263–269
48. Saranathan M, Manojkumar S, Rettmann DW et al (2012) Differential subsampling with Cartesian ordering (DISCO): a high spatio-temporal resolution Dixon imaging sequence for multiphasic contrast enhanced abdominal imaging. J Magn Reson Imaging 35:1484–1492
49. Egbert ND, Bloom DA, Dillman JR (2013) Magnetic resonance imaging of the pediatric pancreaticobiliary system. Magn Reson Imaging Clin N Am 21:681–696
50. Arizono S, Shigeki A, Hiroyoshi I et al (2010) High spatial resolution 3D MR cholangiography with high sampling efficiency technique (SPACE): comparison of 3 T vs. 1.5 T. Eur J Radiol 73:114–118
51. Haystead CM, Dale BM, Merkle EM (2008) N/2 ghosting artifacts: elimination at 3.0-T MR cholangiography with SPACE pulse sequence. Radiology 246:589–595

52. Dickerson EC, Dillman JR, Smith EA et al (2015) Pediatric MR urography: indications, techniques, and approach to review. Radiographics 35:1208–1230
53. Hernando D, Diego H, Levin YS et al (2014) Quantification of liver iron with MRI: state of the art and remaining challenges. J Magn Reson Imaging 40:1003–1021
54. Gandon Y, Olivié D, Guyader D et al (2004) Non-invasive assessment of hepatic iron stores by MRI. Lancet 363:357–362
55. Kim D, Jensen JH, Wu EX et al (2009) Breathhold multiecho fast spin-echo pulse sequence for accurate R2 measurement in the heart and liver. Magn Reson Med 62:300–306
56. St Pierre TG, Clark PR, Chua-anusorn W et al (2005) Noninvasive measurement and imaging of liver iron concentrations using proton magnetic resonance. Blood 105:855–861
57. Tran VT, Vasanawala S (2013) Pediatric hepatobiliary magnetic resonance imaging. Radiol Clin N Am 51:599–614
58. Wood JC (2005) MRI R2 and R2* mapping accurately estimates hepatic iron concentration in transfusion-dependent thalassemia and sickle cell disease patients. Blood 106:1460–1465
59. Robson MD, Gatehouse PD, Bydder M et al (2003) Magnetic resonance: an introduction to ultrashort TE (UTE) imaging. J Comput Assist Tomogr 27:825–846